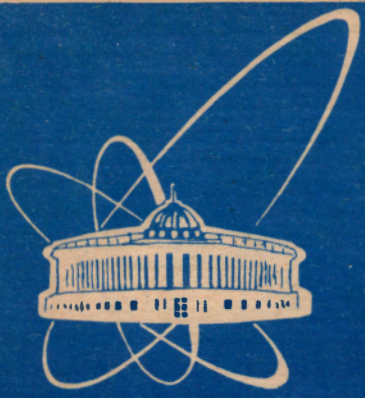

ОБЪЕДИНЕННЫЙ
ИНСТИТУТ
ЯДЕРНЫХ
ИССЛЕДОВАНИЙ

Дубна

E5-97-111

I.V.Barashenkov, Yu.S.Smirnov

COLLECTIVE STATES OF EXTERNALLY DRIVEN, DAMPED NONLINEAR SHRÖDINGER SOLITONS

Submitted to «Physical Review E»

1997

1 Introduction

1.1 Motivation

The present work continues our study of stationary localized solutions of the AC-driven, damped nonlinear Schrödinger equation:

$$i\Psi_t + \Psi_{xx} + 2|\Psi|^2\Psi = -i\gamma\Psi - he^{i\Omega t}. \tag{1}$$

Originally proposed as an amplitude equation for small-amplitude breathers in charge-density-wave materials in the presence of an applied AC field [1], this equation reappeared later in a variety of contexts. Among these are breathers in long Josephson junctions [2] and ferromagnetic chains with an applied microwave field [3], and solitons in the rf-driven plasma [4, 5]. More recently, Eq.(1) was used to describe temporal and spatial soliton propagation in a single-mode fiber ring cavity in the presence of an input forcing beam [6].

It was demonstrated by a simple semiphenomenological argument that solitons of Eq.(1) may bind together to form bound states [7, 8]. Independently, a similar prediction was made on the basis of the adiabatic equations of the Inverse Scattering-based perturbation theory [9]. Subsequently, these bound solitons were observed in direct numerical simulations of the full time-dependent NLS equation (1) [9, 8]. However, the above results are only valid for *small* h and γ, and either do not discriminate between the two solitons (Ψ_+ and Ψ_-) exhibited by Eq.(1) or focus on the stable soliton (Ψ_-) only. The applicability of the collective coordinate approach to the soliton dynamics is not unquestionable either; its main drawback is that it is only applicable to widely separated solitons. It is fitting to note here that our results presented below are not always in agreement with the collective coordinate predictions.

It is the aim of the present work to study bound states in more detail, and without assuming the smallness of h and γ. Since for $\gamma \neq 0$ the system (1) is not conservative, it is not obvious how one could define the binding energy. For this reason we avoid using the term "bound state" and refer to these objects as "collective states", "multisoliton complexes" or simply "multisoliton solutions". By doing this we are trying to emphasize the fact that the multisoliton complexes are not necessarily stable, a property that would be imperative for bound states. We will study a variety of soliton associations: Ψ_- with Ψ_- (we denote this complex $\Psi_{(--)}$); Ψ_+ with Ψ_+ (denoted $\Psi_{(++)}$); $\Psi_{(-+)}$, $\Psi_{(+-+)}$, $\Psi_{(---)}$, $\Psi_{(-+-)}$, $\Psi_{(+++)}$ etc.

This paper has grown out of our attempts to tie up several loose ends left in our previous publication [10]. Those open problems concerned the domain of existence of the Ψ_- soliton for large γ ($\gamma \geq 1/2$). Consequently, in the present article we concentrate on the case of *strongly* damped equations, $\gamma \geq 1/2$. We are planning to return to the case of the weak damping in future publications.

The paper is organized as follows. The next two subsections contain some technical preliminaries: in Sec.1.2 we give explicit formulas for the background flat-locked solution and in Sec.1.3 introduce the bifurcation measure that will be used throughout the paper. Sec.2 is devoted to the bifurcation of the Ψ_- soliton, the problem carried over from the previous paper [10]. For the case of the weak damping, $\gamma \leq 1/2$, we construct the Ψ_+ and Ψ_- solitons as asymptotic series in the vicinity of the upper boundary of their domain of existence. The asymptotic analysis serves to confirm the numerical conclusions of [10], namely that the

Ψ_+ solution merges with the flat background while the Ψ_- goes over to a finite amplitude solution decaying as a power law. Proceeding to the strong damping, $\gamma \geq 1/2$, we report a new phenomenon: instead of becoming a power-law decaying function, the Ψ_- soliton turns into a new branch of three-soliton solutions. This branch appears to be not unique; a host of other localized solutions is presented in Sec.4. Before that we describe a simple variational formalism (Sec.3) which is then used to identify different localized solutions as two- and three-soliton complexes. Our key result is the bifurcation diagram Fig.5 illustrating links and relationships between all soliton complexes obtained so far.

1.2 Flat Background

As in [10] we fix, without loss of generality, $\Omega = 1$ and make the transformation $\Psi(x,t) = e^{it}\psi(x,t)$, reducing Eq.(1) to an autonomous equation

$$i\psi_t + \psi_{xx} - \psi + 2|\psi|^2\psi = -i\gamma\psi - h. \tag{2}$$

The advantage is that we will be able to deal with time-independent solutions instead of periodic ones. The time-independent solutions of Eq.(2) satisfy

$$\psi_{xx} - \psi + 2|\psi|^2\psi = -i\gamma\psi - h; \tag{3}$$

this is the equation that we are going to study in this paper. We first recall briefly some facts about the *flat-locked* (or continuous-wave) solutions to Eq.(1), i.e. homogeneous solutions of Eq.(3). It is convenient to decompose ψ_0 as $\psi_0 = \sqrt{\rho_0}\exp(i\theta)$; then

$$\tan\theta = \frac{\gamma}{1-2\rho_0}, \quad 0 \leq \theta \leq \pi,$$

and ρ_0 is a root of the following cubic equation:

$$4\rho_0^3 - 4\rho_0^2 + (1+\gamma^2)\rho_0 - h^2 = 0. \tag{4}$$

Approximate [5, 11] and numerical [12] solutions of Eq.(4) are available for small h and γ. The analysis for general h and γ is presented in our previous publication [10]. Although we did not write out explicit formulas for the roots, we identified regions of characteristic behaviour of the roots on the (h,γ)-plane, and gave analytic expressions for boundaries between these regions. In fact, explicit solutions can be easily found in reference books; we list them here since they prove useful in calculations.

An explicit formula for the roots is written in terms of coefficients of the associated incomplete cubic equation,

$$y^3 + Py + Q = 0,$$

where $y = \rho_0 - 1/3$, and the coefficients are given by

$$P = \frac{1}{4}\left(\gamma^2 - \frac{1}{3}\right),$$

and

$$Q = \frac{1}{12}\left(\gamma^2 + \frac{1}{9} - 3h^2\right).$$

The number of real (positive) roots varies with h and γ. Two characteristic regions of γ can be identified as follows.

First, when $\gamma \leq 1/\sqrt{3}$, the coefficient P is negative, and Eq.(4) may have three or one real positive root, depending on how h compares with h_+ and h_-, where

$$h_\pm = h_\pm(\gamma) = \left\{\tfrac{1}{3}(\gamma^2+\tfrac{1}{9}) \pm \tfrac{1}{3}\sqrt{\tfrac{1}{3}\left(\tfrac{1}{3}-\gamma^2\right)^3}\right\}^{1/2}. \tag{5}$$

If h is greater than h_+ or smaller than h_-, the discriminant of Eq.(4),

$$\mathcal{D} = -108\left\{\left(\frac{P}{3}\right)^3 + \left(\frac{Q}{2}\right)^2\right\}, \tag{6}$$

is negative and the equation has only one real root:

$$\rho_0 \doteq \frac{1}{3} - 2\left(-\frac{P}{3}\right)^{1/2}\frac{1}{\sin 2\alpha},$$

where

$$\tan\alpha = \left(\tan\frac{\beta}{2}\right)^{1/3} \quad \left(|\alpha| \leq \frac{\pi}{4}\right),$$

and

$$\sin\beta = \frac{2}{Q}\left(-\frac{P}{3}\right)^{3/2} \quad \left(|\beta| \leq \frac{\pi}{2}\right).$$

Here positive values of Q, α and β correspond to $h < h_-$ and

$$\rho_0 < \frac{1}{3} - \frac{1}{3}\sqrt{1-3\gamma^2}.$$

Negative Q, α and β pertain to $h > h_+$ and

$$\rho_0 > \frac{1}{3} + \frac{1}{3}\sqrt{1-3\gamma^2}.$$

If $\gamma \leq 1/\sqrt{3}$ and h falls between h_- and h_+, the discriminant (6) is positive and there are three positive roots, $0 < \rho_0^{(1)} < \rho_0^{(2)} < \rho_0^{(3)}$:

$$\rho_0^{(1)} = \frac{1}{3} - 2\left(-\frac{P}{3}\right)^{1/2}\cos\left(\frac{\alpha}{3} - \frac{\pi}{3}\right),$$

$$\rho_0^{(2)} = \frac{1}{3} - 2\left(-\frac{P}{3}\right)^{1/2}\cos\left(\frac{\alpha}{3} + \frac{\pi}{3}\right),$$

$$\rho_0^{(3)} = \frac{1}{3} + 2\left(-\frac{P}{3}\right)^{1/2}\cos\frac{\alpha}{3},$$

where

$$\cos\alpha = -\frac{Q/2}{(-P/3)^{3/2}} \quad (0 \le \alpha \le \pi).$$

It is not difficult to find the ranges of the above roots:

$$\frac{1}{3} - \frac{1}{3}\sqrt{1-3\gamma^2} \le \rho_0^{(1)} \le \rho_-(\gamma);$$

$$\rho_-(\gamma) \le \rho_0^{(2)} \le \rho_+(\gamma);$$

$$\rho_+(\gamma) \le \rho_0^{(3)} \le \frac{1}{3} + \frac{1}{3}\sqrt{1-3\gamma^2},$$

where

$$\rho_\pm(\gamma) = \frac{1}{3} \pm \frac{1}{6}\sqrt{1-3\gamma^2}. \tag{7}$$

In the **second** region, when $\gamma \ge 1/\sqrt{3}$, the coefficient P is positive, discriminant negative and we only have one real (positive) root:

$$\rho_0 = \frac{1}{3} - 2\left(\frac{P}{3}\right)^{1/2}\cot 2\alpha,$$

where

$$\tan\alpha = \left(\tan\frac{\beta}{2}\right)^{1/3} \quad \left(|\alpha| \le \frac{\pi}{4}\right),$$

and

$$\tan\beta = \frac{2}{Q}\left(\frac{P}{3}\right)^{3/2} \quad \left(|\beta| \le \frac{\pi}{2}\right).$$

This completes the description of the flat solutions of Eq.(3).

1.3 Bifurcation measure

In order to describe transformations and bifurcations of solutions to Eq.(3) quantitatively, we need a real-valued functional which would represent solutions as points in R^1. In our previous publication [10] we used the value $|\psi(0)|^2$ as a bifurcation measure. The disadvantage of this measure is that it is very sensitive to numerically-induced shifts of the solution as a whole: $\psi(x) \to \psi(x - x_0)$. Also it completely disregards the variation of the soliton's shape away from the point $x = 0$ while it is the soliton's "wings" that change most significantly as new solitons attach to the multisoliton state. For these and some other reasons which will become clear below, we find it useful to replace the single-point measure by an integral characteristic of solutions.

Using Eq.(2) it is straightforward to verify the following relation:

$$\frac{dE}{dt} + 2\gamma E = 2\gamma\int\left\{|\psi|^4 - \frac{h}{2}(\psi+\overline{\psi}) - |\psi_0|^4 + \frac{h}{2}(\psi_0+\overline{\psi}_0)\right\}dx, \tag{8}$$

where

$$E = \int \left\{|\psi_x|^2 + |\psi|^2 - |\psi|^4 - h(\psi+\overline{\psi}) - |\psi_0|^2 + |\psi_0|^4 + h(\psi_0+\overline{\psi}_0)\right\}dx. \tag{9}$$

When $\gamma = 0$, the quantity E is conserved and represents the energy of the system. In this case it is a natural candidate for the bifurcation measure. We have found it useful to retain E Eq.(9) as a bifurcation measure even in the case $\gamma \ne 0$, when it is not conserved. Although the meaning of this quantity is not so obvious now, we will still be referring to E as energy.

When ψ is a time-independent solution, we have $dE/dt = 0$ and Eq.(8) gives a useful representation for the energy of static solutions:

$$E = \int \left\{|\psi|^4 - \tfrac{h}{2}(\psi+\overline{\psi}) - |\psi_0|^4 + \tfrac{h}{2}(\psi_0+\overline{\psi}_0)\right\}dx. \tag{10}$$

2 Bifurcation of the ψ_- soliton

We start with returning to a question remained unanswered in our previous publication [10]. There, we attempted to find, numerically, the upper boundary of the domain of existence of the ψ_+ and ψ_- solitons.

2.1 Types of the asymptotic decay

In order to find the upper boundary, it is useful to consider first the asymptotic region, $|x| \to \infty$. The solitons decay to the value ψ_0 exponentially:

$$\psi_\pm(x) - \psi_0 \sim e^{(-p+ik)|x|} \quad \text{as} \quad |x| \to \infty,$$

where $p, k > 0$ and the complex exponent $\kappa = -p + ik$ satisfies [10]

$$(\kappa^2)_{1,2} = 1 - 4|\psi_0|^2 \pm \sqrt{4|\psi_0|^4 - \gamma^2}. \tag{11}$$

Both $(\kappa^2)_{1,2}$ are negative for certain $|\psi_0|^2$ and hence there can be no solitons with these asymptotic values. In the region $\gamma > 1/\sqrt{3}$ this happens for $|\psi_0|^2 > \gamma/2$; in the region $1/2 < \gamma < 1/\sqrt{3}$ both κ^2 are negative for $\gamma/2 < |\psi_0|^2 < \rho_-$ and for $|\psi_0|^2 > \rho_+$; finally, in the region $\gamma < 1/2$ this situation takes place for $|\psi_0|^2 > \rho_+$. Next, when $|\psi_0|^2$ lies between ρ_- and ρ_+ (where ρ_- and ρ_+ are as in Eq.(7)), one root $(\kappa^2)_1$ is positive and the other one $(\kappa^2)_2$ negative. There can, in principle, exist solutions with such asymptotic values. However, none were found [10]. Furthermore, flat solutions with $\rho_- < |\psi_0|^2 < \rho_+$ are unstable [10], and hence these solitons would be of little interest even if existed.

There are two ranges of $|\psi_0|^2$ where solitons can exist. The first one is $|\psi_0|^2 < \gamma/2$ (for all γ). Here both $(\kappa^2)_{1,2}$ are complex yielding nonzero p and k. The solitons undergo an oscillatory decay to the flat background, with the decay rate

$$p^2 = \frac{1 - 4|\psi_0^2|}{2} + \frac{\sqrt{(1-4|\psi_0|^2)^2 + \gamma^2 - 4|\psi_0|^4}}{2}, \tag{12}$$

and the wavenumber of undulations

$$k = \frac{\sqrt{\gamma^2 - 4|\psi_0|^4}}{2p}. \tag{13}$$

For $\gamma < 1/2$ there is also another range: $\gamma/2 < |\psi_0|^2 < \rho_-$. Here both κ^2 are positive, and solitons approach their asymptotic values monotonically ($k = 0$), with the decay exponent

$$p^2 = 1 - 4|\psi_0|^2 - \sqrt{4|\psi_0|^4 - \gamma^2}. \tag{14}$$

The inequality $|\psi_0|^2 < \gamma/2$ can be rewritten as $h < h_*(\gamma)$ where

$$h_*(\gamma) \equiv (\gamma^3 - \gamma^2 + \gamma/2)^{1/2}, \tag{15}$$

and now we can summarise our conclusions in terms of h and γ: For small γ, $\gamma < 1/2$, the ψ_+ and ψ_- solitons can only exist for $h < h_+$. They exhibit two types of asymptotic decay: monotonic for $h_* < h < h_+$ and oscillatory for $h < h_*$. The corresponding decay rates are given by Eqs.(14) and (12), respectively. On the contrary, in the region $\gamma > 1/2$ the decay is always oscillatory. Here there can be no localized solutions above the value $h = h_*$. For $h < h_*$, the decay exponent is given by Eq.(12) and the wavenumber of the asymptotic undulations by Eq.(13).

2.2 Weak damping, $\gamma < 1/2$

Now we are prepared to discuss soliton transformations in the vicinity of the upper boundary. Assume γ is smaller than $1/2$ and fixed. As h increases to the value h_+, where $h_+(\gamma)$ is given by Eq.(5), the decay exponent p, Eq.(14), goes to zero. The fate of the two solitons, ψ_+ and ψ_- turns out to be different.

The amplitude of the ψ_+ soliton was observed to decrease while its characteristic width was increasing and eventually the ψ_+ was seen to merge with the flat solution: $\psi_+(x) \to \psi_0$ as $h \uparrow h_+$. On the contrary, the soliton ψ_- retained a finite amplitude and remained well localised in this limit (though the decay exponent p did tend to zero). We were able to obtain this solution in a very near vicinity of the point h_+. (More precisely, we were able to find the ψ_- with the asymptotic value $|\psi_0|^2$ deviating not more than by 10^{-3} from the curve $\rho_-(\gamma)$. In terms of h, this means that the upper boundary is given by $h_+(\gamma)$ to within the accuracy of order 10^{-6}.) This implies that as $h \to h_+$, the soliton ψ_- transforms into a localised solution decaying as a power of x. (There is a very subtle question of whether the ψ_- exists *arbitrarily* close to h_+, i.e whether this power-law decaying solution is actually reached. This point is discussed in section 5.)

These numerical observations can be substantiated by constructing the solitons ψ_+ and ψ_- as asymptotic series for $h \to h_+$. Letting $\psi(x) = \psi_0(x)[1 + \delta\chi(x)]$, substituting into eq.(2) and keeping up to quadratic terms in $\delta\chi = u + iv$, yields

$$L \begin{pmatrix} u \\ v \end{pmatrix} = \begin{pmatrix} u_{xx} \\ v_{xx} \end{pmatrix} + 2|\psi_0|^2 \begin{pmatrix} 3u^2 + v^2 \\ 2uv \end{pmatrix}, \tag{16}$$

where the matrix

$$L = \begin{pmatrix} 1 - 6|\psi_0|^2 & \gamma \\ -\gamma & 1 - 2|\psi_0|^2 \end{pmatrix}. \tag{17}$$

Assume that h approaches h_+ from below; then we can define a small parameter ϵ^2 by

$$|\psi_0|^2 = \rho_-(\gamma) - \epsilon^2. \tag{18}$$

Using (18), the matrix L reads

$$L = \begin{pmatrix} \sqrt{1 - 3\gamma^2} - 1 & \gamma \\ -\gamma & \frac{1}{3} + \frac{1}{3}\sqrt{1 - 3\gamma^2} \end{pmatrix} + \epsilon^2 \begin{pmatrix} 6 & 0 \\ 0 & 2 \end{pmatrix} \equiv$$
$$\equiv L_0 + \epsilon^2 L_1. \tag{19}$$

For h close enough to h_+ (more precisely, for h between h_* and h_+) the deviation $\delta\chi(x)$ decays as $e^{-p|x|}$, with the positive exponent p being given by Eq.(14). As $|\psi_0|^2 \uparrow \rho_-$, p tends to zero. Using (18), one finds

$$p^2 = \frac{6\sqrt{1 - 3\gamma^2}}{2\sqrt{1 - 3\gamma^2} - 1}\epsilon^2,$$

that is, $p \sim \epsilon$. Consequently, we expand the small deviation $\delta\chi$ as

$$\begin{pmatrix} u(x) \\ v(x) \end{pmatrix} = \epsilon^2 \begin{pmatrix} u_1(z) \\ v_1(z) \end{pmatrix} + \epsilon^4 \begin{pmatrix} u_2(z) \\ v_2(z) \end{pmatrix} + \dots, \tag{20}$$

where $z = \epsilon x$. Substituting into eq.(16) and equating the coefficient at the power ϵ^2 to zero yields

$$L_0 \begin{pmatrix} u_1 \\ v_1 \end{pmatrix} = 0, \tag{21}$$

or, equivalently,

$$v_1(x) = \mu u_1(x), \tag{22}$$

where

$$\mu = \frac{1 - \sqrt{1 - 3\gamma^2}}{\gamma}.$$

Next, at the order ϵ^4 we get

$$L_0 \begin{pmatrix} u_2 \\ v_2 \end{pmatrix} = \left(\frac{d^2}{dz^2} - L_1\right) \begin{pmatrix} u_1 \\ v_1 \end{pmatrix} + \rho_- \begin{pmatrix} 3u_1^2 + v_1^2 \\ 2u_1 v_1 \end{pmatrix}. \tag{23}$$

This system of two linear algebraic equations is only solvable if the right-hand side is orthogonal to the vector $(u_1, -v_1)$ in the sense of the R^2-scalar product. (The vector $(u_1, -v_1)$ is the zero-eigenvalue eigenvector of the conjugate matrix L_0^+.) This condition gives

$$(1 - \mu^2)\frac{d^2 u_1}{dz^2} - 2(3 - \mu^2)u_1 + 2\rho_-(3 - \mu^2)u_1^2 = 0, \tag{24}$$

where we have made use of (19) and (22). Since, as one can easily check, μ is smaller than 1, the quantity

$$\frac{2(1 - \mu^2)}{3 - \mu^2} = z_0^2$$

is positive and we have two solutions of eq.(24) :

$$u_1^+ = \frac{3}{2\rho_-}\frac{1}{\cosh^2(z/z_0)},$$
$$u_1^- = -\frac{3}{2\rho_-}\frac{1}{\sinh^2(z/z_0)}.$$

These give rise to two different perturbations $\delta\chi$:

$$\delta\chi^+ = \frac{3(1+i\mu)}{2\rho_-}\frac{\epsilon^2}{\cosh^2(\epsilon x/z_0)} + O(\epsilon^4),$$

$$\delta\chi^- = -\frac{3(1+i\mu)}{2\rho_-}\frac{\epsilon^2}{\sinh^2(\epsilon x/z_0)} + O(\epsilon^4).$$

The function $\delta\chi^+$ is bounded for all x and so this perturbation of the flat background yields a true nonlinear solution valid for all x. As $\epsilon \to 0$, this solution merges with the flat background and therefore, is nothing but the soliton ψ_+.

The function $\delta\chi^-$ grows indefinitely as $x \to 0$; hence this perturbation gives only an asymptotic approximation of the solution, valid for large $|x| >> z_0$. The asymptotic series (20) does not have to converge for all x. For those sufficiently large x where it does converge, the asymptotic solution $\psi_0(1+\delta\chi^-)$ should be identified with the ψ_- soliton. Sending $\epsilon \to 0$ for a fixed x, one gets

$$\delta\chi^- \to -\frac{3(1+i\mu)}{2\rho_-}\frac{z_0^2}{x^2} + O(\epsilon^2).$$

Thus, when h tends to the value h_+, the ψ_- soliton should approach a finite-amplitude solution with a power-law decay.

2.3 $\gamma = 0$: explicit solution

As an illustration to the asymptotic and numerical analysis we consider the case $\gamma = 0$. In this case we have a pair of explicit solutions [13]:

$$\psi_\pm(x) = \psi_0\left(1 + \frac{2\sinh^2\alpha}{1 \pm \cosh\alpha\cosh Ax}\right), \tag{25}$$

where α is defined by the magnitude of the driver:

$$h = \frac{\sqrt{2}\cosh^2\alpha}{(1+2\cosh^2\alpha)^{3/2}}, \tag{26}$$

and ψ_0 and A are given by

$$\psi_0 = \frac{1}{\sqrt{2(1+2\cosh^2\alpha)}} > 0,$$
$$A = 2\psi_0\sinh\alpha = \sqrt{1-6\psi_0^2} = \frac{\sqrt{2}\sinh\alpha}{\sqrt{1+2\cosh^2\alpha}}. \tag{27}$$

Let now $h \to h_+ = \sqrt{2/27}$ or, equivalently, $\alpha \to 0$. In agreement with the predictions of the asymptotic analysis, the ψ_+ soliton goes over to the flat solution while the ψ_- becomes a rational function:

$$\psi_-(x) \to \frac{1}{\sqrt{6}}\frac{2x^2-9}{2x^2+3}. \tag{28}$$

These transformations are reflected by the behaviour of the energy. Substituting (2.3) into eq.(10), the energy of the solitons $\psi_\pm$ is given by

$$E^+ = E[\psi_+] = \frac{8}{\sqrt{2}}\frac{\sinh\alpha + \frac{2}{3}\sinh^2\alpha - \beta\cosh^2\alpha}{(1+2\cosh^2\alpha)^{3/2}}, \tag{29}$$

$$E^- = E[\psi_-] = E^+ + \frac{8\pi}{\sqrt{2}}\frac{\cosh^2\alpha}{(1+2\cosh^2\alpha)^{3/2}}, \tag{30}$$

where

$$\beta = \arccos\left(\frac{1}{\cosh\alpha}\right).$$

As $h \to h_+$ ($\alpha \to 0$), the energy of the ψ_+ tends to the energy of the flat solution (i.e. to zero):

$$E^+ = C(h_+ - h)^{5/4} + O\left((h_+ - h)^{7/4}\right), \tag{31}$$

with $C = (16/5)2^{1/8}3^{5/8} \approx 6.934$. On the contrary, the energy of the ψ_- soliton tends to a finite value which indicates that the ψ_- does not flatten out but approaches a localized solution with a power-law decay:

$$E^- = \frac{8\pi}{3\sqrt{6}} - 4\pi(h_+ - h) + O\left((h_+ - h)^{5/4}\right). \tag{32}$$

2.4 Strong damping, $\gamma \geq 1/2$

The situation in the region $\gamma \geq 1/2$ turns out to be more complicated. In this region the decay rate is given by Eq.(12); as we mentioned in subsection 2.1, it goes to zero as $h \to h_*$ and $|\psi_0|^2 \to \gamma/2$. Similarly to the case $\gamma < 1/2$, the ψ_+ soliton was observed to merge with the flat solution here. (We were able to find the ψ_+ arbitrarily close to the value $h = h_*$). It was natural to expect the ψ_- soliton to behave similarly to the $\gamma < 1/2$ case as well. As we have already mentioned, in the region $\gamma \leq 1/2$ we were able to find the ψ_- soliton with the asymptotic value $|\psi_0|^2$ deviating from the curve $\rho_-(\gamma)$ not more than by 10^{-3}. On the contrary, when $\gamma > 1/2$, the upper boundary was found to digress quite substantially from $|\psi_0|^2 = \gamma/2$. It has remained unclear in Ref.[10] what causes this digression and what finally happens to the ψ_- soliton as h increases.

In order to clarify the situation, we have designed a sixth-order numerical algorithm based on the continuous analog of Newton's method and performed an accurate study of the neighbourhood of the point $h = h_*$. (For references and a brief review of the method, see [10].) Results of this study are presented in Figs.1-3. This more accurate analysis revealed that the reason why we were not able to approach the point $h = h_*$ close enough in Ref.[10], was the existence of a new turning point. At this point the ψ_- branch turns into a new

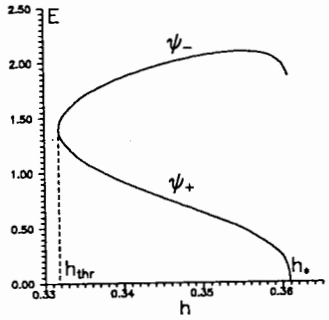

Fig.1 The bifurcation diagram of the one-soliton solution for $\gamma = 0.52$. At the point $h = h_* = 0.360843$ (where $|\psi_0|^2 = \gamma/2 = 0.26$) the soliton ψ_+ detaches from the flat solution (whose energy is zero.) The point $h_{\rm thr} = 0.3318065$ is a turning point; at this point the ψ_+ soliton transforms into the ψ_- solution. The ψ_- soliton ceases to exist for $h > 0.3607921$ or, speaking in terms of the asymptotic values, for $|\psi_0|^2 > 0.2544168$. The question of what happens for h between $h = 0.3607921$ and $h_* = 0.360843$, was left open in the previous publication [10].

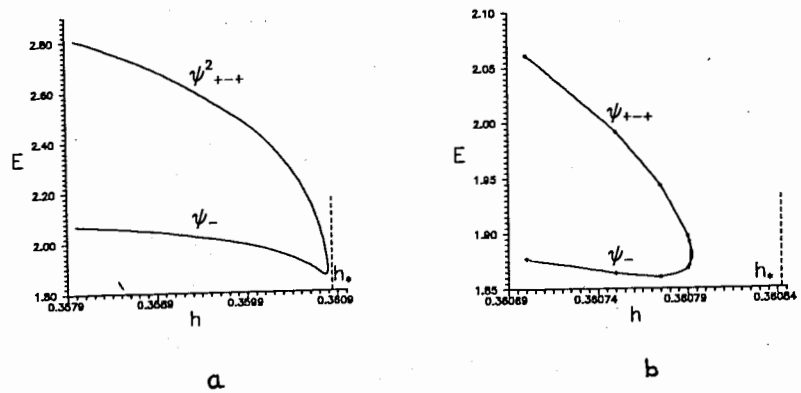

Fig.2 Bifurcation to a three-soliton complex for $\gamma = 0.52$. Two parts of this figure show a small neighbourhood of the point h_*. The lower curve is the last segment of the ψ_- branch from Fig.1. The solution corresponding to the upper curve is plotted in Fig.3. The part b is an enlarged portion of the part a next to the turning point.

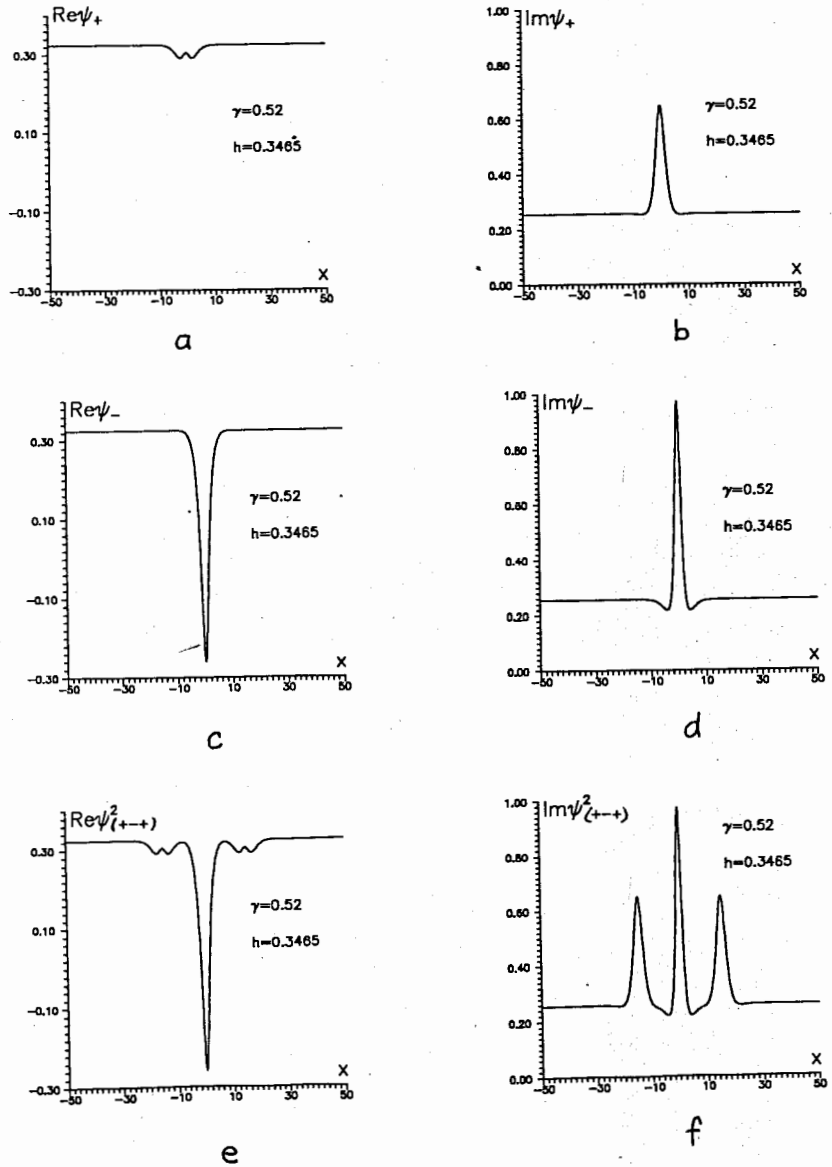

Fig.3 Localised solutions corresponding to the three branches of the bifurcation diagram in Figs. 1 and 2. a,b) ψ_+, the lowest branch; c,d) ψ_-, the middle branch; e,f) a new branch into which the ψ_- branch turns at the point $h = 0.3607921$. It is quite obvious from the comparison of the three sets of pictures that the last solution is a combination of "psi-minus" and two "psi-pluses". (Below we call this complex $\psi^2_{(+-+)}$.) In these pictures, $\gamma = 0.52$ and $h = 0.3465$.

branch of localised solutions, see Fig.3 Solutions of this branch are nonlinear superpositions of three solitons: ψ_- soliton in the middle and two ψ_+ solitons at its sides.

A more extensive search revealed the existence of a larger variety of multisoliton complexes. The corresponding energies are plotted in Fig.5 below (Sec.4.) Before proceeding to the description of the resulting bifurcation diagram, we introduce a simple variational formalism which will allow us to identify its various branches.

3 Collective coordinate description

We now present a simple semiphenomenological argument for the existence of soliton complexes, which would also allow to estimate their separation distances. It is convenient to consider three-soliton configurations first; the two-soliton state will be obtainable as a simple particular case. We set up a trial function in the form of a linear combination

$$\psi_1\psi_2\psi_3(x;z) \equiv \psi_1 + \psi_2 + \psi_3 - 2\psi_0, \tag{33}$$

where

$$\psi_1 = \psi_1(x+z), \quad \psi_2 = \psi_2(x), \quad \psi_3 = \psi_3(x-z)$$

are three different or identical solitons sitting at the points $x = -z, 0$ and $+z$, respectively. Here z is a positive value that is allowed to depend on time: $z = z(t)$. We have to use a bit awkward notation $\psi_1\psi_2\psi_3$ in order to distinguish the *linear combination* of three solitons from the *genuine three-soliton solution*; our notation for the latter would be $\psi_{(123)}$.

The damped driven NLS equation (1) follows from the stationary action principle $\delta S = 0$, where

$$S = \int e^{2\gamma t} L\left[\psi, \overline{\psi}\right] dt \tag{34}$$

and the Lagrangian

$$L = T - E \tag{35}$$

comprises the kinetic

$$T = \frac{i}{2}\int_{-\infty}^{\infty} \left(\psi_t\overline{\psi} - \overline{\psi}_t\psi\right) dx \tag{36}$$

and "potential" term

$$E = \int \begin{array}{l} \left\{|\psi_x|^2 + |\psi|^2 - |\psi|^4 - h(\psi + \overline{\psi}) - \right. \\ \left. -|\psi_0|^2 + |\psi_0|^4 + h(\psi_0 + \overline{\psi}_0)\right\} dx. \end{array} \tag{37}$$

Substituting the Ansatz (33) into Eqs.(35)-(37), we obtain for the kinetic term

$$T = T_{11} + T_{33} + T_{13} + T_{12} + T_{23}, \tag{38}$$

where

$$T_{11} = \frac{i}{2}\dot{z}\int \left\{\frac{d\psi_1}{dx}(\overline{\psi}_1 - \overline{\psi}_0) - c.c.\right\} dx, \tag{39}$$

$$T_{33} = -\frac{i}{2}\dot{z}\int \left\{\frac{d\psi_3}{dx}(\overline{\psi}_3 - \overline{\psi}_0) - c.c.\right\} dx, \tag{40}$$

$$T_{13} = \frac{i}{2}\dot{z}\int \left\{\left(\frac{d\psi_1}{dx}\overline{\psi}_3 + \psi_1\frac{d\overline{\psi}_3}{dx}\right) - c.c.\right\} dx = \\ = \frac{i}{2}\dot{z}\left(\psi_1\overline{\psi}_3 - \psi_3\overline{\psi}_1\right)\Big|_{-\infty}^{+\infty}, \tag{41}$$

and

$$T_{12} + T_{23} = \frac{\dot{z}}{2}\frac{d\sigma}{dz}$$

with

$$\sigma(z) = i\int \left\{\left(\overline{\psi}_2 - \overline{\psi}_0\right)\left(\psi_1 + \psi_3\right) - c.c.\right\} dx. \tag{42}$$

In the above formulas, $\psi_1 = \psi_1(x+z)$, $\psi_2 = \psi_2(x)$, and $\psi_3 = \psi_3(x-z)$. The terms T_{11} and T_{33} vanish because $\psi_1(x)$ and $\psi_3(x)$ are even functions, and $T_{13} = 0$ because ψ_1 and ψ_3 approach the same value ψ_0 at the plus and minus infinity.

We now have

$$L = \frac{\dot{z}}{2}\frac{d\sigma}{dz} - E(z),$$

where $E = E[\psi_1\psi_2\psi_3(x;z)]$ is the functional (37) evaluated at the linear combination (33). Varying the action (34) yields

$$\frac{d}{dz}(E + \gamma\sigma) \equiv \frac{dU_{\text{eff}}}{dz} = 0. \tag{43}$$

Eq.(43) is of the form of a constraint; it describes only stationary solutions. We could have easily made it dynamical just by adding one more time-dependent variable (the canonically-conjugate momentum), but since we are only interested in stationary configurations, Eq.(43) is quite sufficient for our purposes.

In the three-soliton case, we confine ourselves to *symmetric* configurations and assume that $\psi_1(x) = \psi_3(x)$. In this case the Ansatz (33) describes two identical solitons ψ_1 (which can be either two ψ_+'s or two ψ_-'s) placed at the distance $2z$ from one another, and an additional soliton ψ_2 sitting symmetrically in between. The intermediate soliton can be of the same variety as the two side ones (like in $\psi_{(+++)}$) or of the different kind (e.g. $\psi_{(+-+)}$). Notice that the function

$$\psi_1 + \psi_3 = \psi_1(x+z) + \psi_1(x-z)$$

is even and so the term $T_{12} + T_{23}$ does not necessarily have to be equal to zero.

The two-soliton case arises if we eliminate the middle soliton by letting $\psi_2(x) \equiv \psi_0$; then the quantity σ vanishes. In this case we do not need to assume that $\psi_1(x) = \psi_3(x)$: ψ_1 and ψ_3 can stand for any combination of ψ_+ and ψ_- solitons. The Euler-Lagrange equation (43) reduces simply to

$$\frac{dE}{dz} = 0. \tag{44}$$

This is almost the same variational principle as the one employed in [7, 8] (see also [14].) The only difference is that we are using the total energy (37) while the authors of [7, 8]

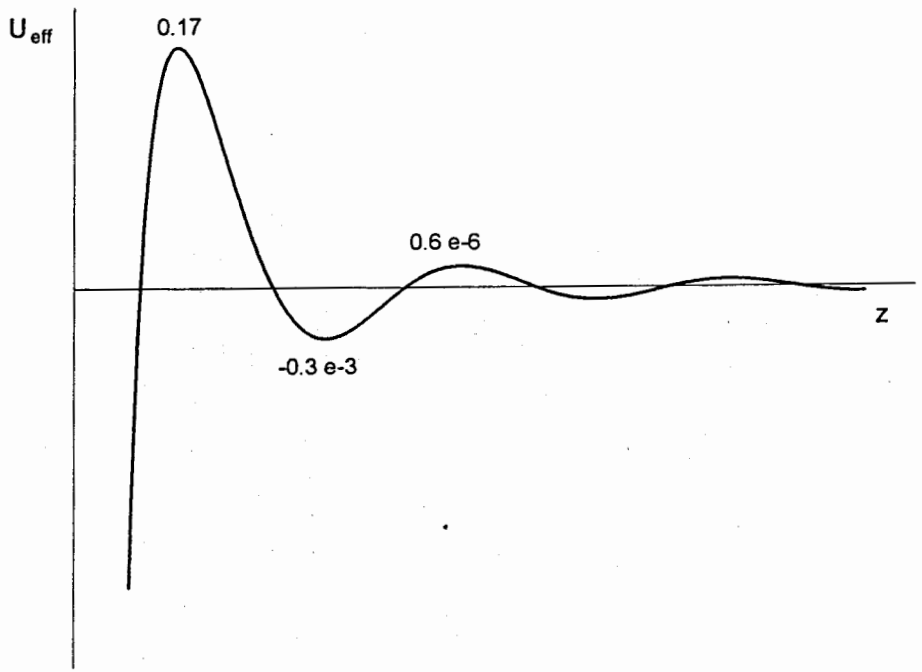

Fig.4 The energy of the two-soliton linear combination $\psi_-\psi_- = \psi_-(x+z) + \psi_-(x-z) - \psi_0$, as a function of the intersoliton separation, $2z$. The energies of the other two-soliton linear combinations, $\psi_+\psi_+$ and $\psi_-\psi_+$, as well as of four symmetric three-soliton superpositions ($\psi_+\psi_+\psi_+, \psi_-\psi_-\psi_-, \psi_+\psi_-\psi_+$ and $\psi_-\psi_+\psi_-$) look qualitatively similar.

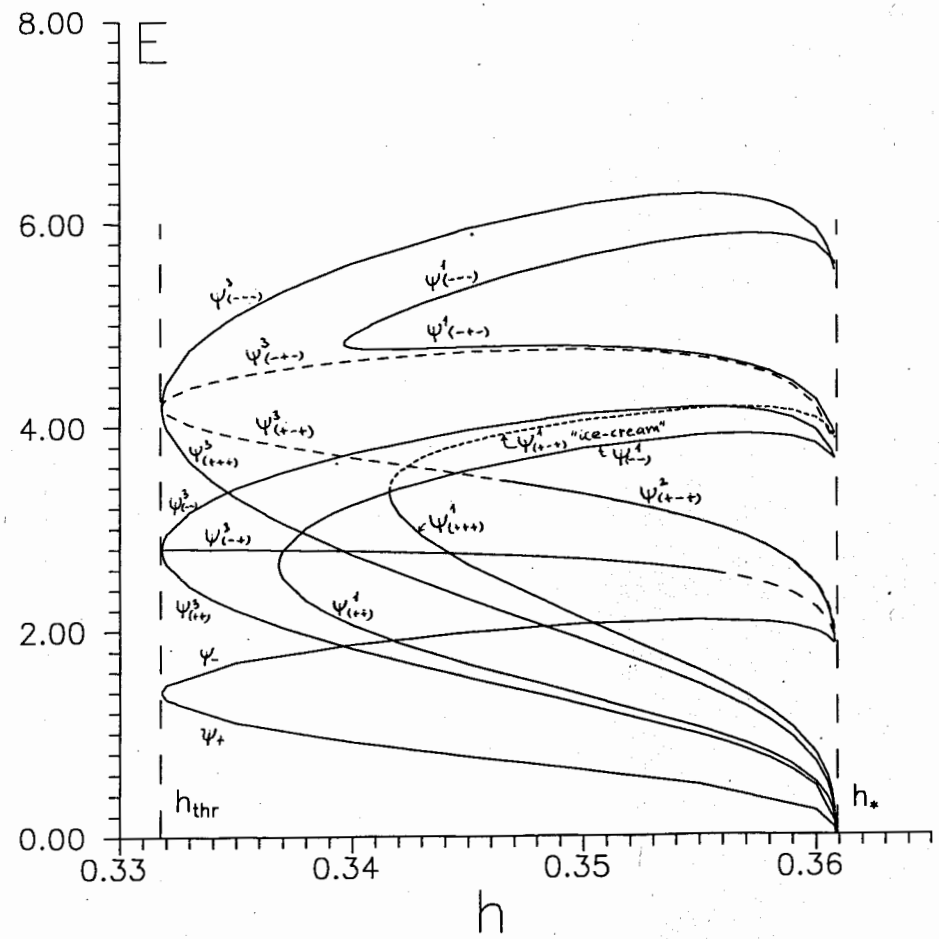

Fig.5 The bifurcation diagram featuring single-soliton, two-soliton and symmetric three-soliton solutions. **1.** Notice that the branch $\psi^3_{(-+)}$, departing from the triple turning point as a solid line, becomes dashed as it continues to the right. This is meant to indicate that we had to relax the residual of the numerical scheme as we advanced in the direction of larger h. We were unable to compute the solution at the dashed section with the residual δ less than $\sim 10^{-6}$ -10^{-5}. **2.** The branch $\psi^2_{(+-+)}$ (solid curve into which the branch ψ_- turns near the value $h = h_*$) terminates at $h \approx 0.3465$; we were unable to advance it further to the left. This solid curve partially conceals the branch $\psi^3_{(+-+)}$ (second dashed curve from the bottom). The latter starts at about the same point as the curve $\psi^2_{(+-+)}$ but extends all way to the quartic turning point where it turns into the $\psi^3_{(-+-)}$. For those h where the complex $\psi^2_{(+-+)}$ exists, the energies of the two orbits, $\psi^2_{(+-+)}$ and $\psi^3_{(+-+)}$, are graphically indistinguishible.

utilised only the interaction term $\int |\psi|^4 dx$. For small h and γ this difference is unessential, but for larger values of these parameters there can be quantitative deviations.

For small h and γ the solitons can be approximated by explicit formulas. In this case, assuming a wide separation between the two solitons the integral (37) can be evaluated analytically [7, 8] and the equation (44) has a sequence of roots ("two-soliton orbits"), z_n:

$$2z_n = \frac{\pi}{2k}(2n-1), \quad n = 1, 2, 3, ..., \tag{45}$$

where k is the soliton's asymptotic wavenumber:

$$\psi(x) - \psi_0 \sim e^{(-p+ik)|x|} \quad \text{as} \quad |x| \to \infty.$$

The above expression applies uniformly to all three two-soliton linear combinations ($\psi_+\psi_+$, $\psi_-\psi_-$ and $\psi_-\psi_+$.) Although eq.(45) was derived for small h and γ only, the general argument behind this result is more general. It simply states that when two solitons are widely separated, the first soliton is only affected by the *tail* of the second one, and since the tails have undulations, the potential of interaction exhibits alternating minima and maxima [7, 8]. Consequently, eq.(45) with k defined by Eq.(12)-(13) can be used as an estimate for the two-soliton orbits for not only very small h and γ.

4 Multisoliton bifurcation diagram

Using the numerically precomputed solitons ψ_- and ψ_+, we have evaluated the effective potential of interaction $U_{\text{eff}} = E + \gamma\sigma$ for all three two-soliton and all four symmetric three-soliton combinations. The potential is shown, as a function of the inter-soliton separation z, in Fig.4. This particular figure corresponds to the $\psi_-\psi_-$ linear combination; however, for all other two and three-soliton combinations the potential looks qualitatively similar. The potential of the soliton-soliton interaction is attractive at short distances, and then intervals of attraction and repulsion alternate. As in the previous section, the consecutive points of extrema are denoted by z_n: z_1 is a maximum, z_2 a minimum and so on. A reservation that we have to make here is that it is only for sufficiently large intersoliton separations that the energy U_{eff} of the above linear combinations yields the true potential of the soliton-soliton interaction.

The positions of the first three extrema obtained in this way, are given in Table 1 (second column). In the first column of this table we give the genuine values of the inter-soliton separation, i.e. the separations exhibited by the numerical solutions of Eq.(3). (Notice that in the two-soliton case, the separation distance between the solitons is $2z$ not z.) Finally, the third column contains the separation distances as obtained by the approximate formula (45).

4.1 Two-soliton complexes

Numerically we were able to find five different two-soliton complexes: four symmetric and one asymmetric. First of all, as depicted in Fig.5, two distinct two-ψ_+ soliton solutions detach from the flat solution at $h = h_*$. These two complexes are only different in their

intersoliton separation distances (Fig.6). For the driver's strength $h = 0.35$ (which will be used as a reference value throughout the paper), the corresponding separations are $2z_1 \approx 7.60$ and $2z_3 \approx 28.00$. By comparing to the predictions of the variational analysis (which gives $2z_1 = 7.95$, $2z_2 = 18.20$ and $2z_3 = 28.45$, see Table 1) one of these solutions can be identified with the first orbit (we denote it $\psi^1_{(++)}$) and the other with the *third*, to be denoted $\psi^3_{(++)}$. (Hence the notation, z_1 and z_3.) Surprisingly, we were not able to find, numerically, the two-ψ_- soliton complex with the solitons sitting at the *second* orbit, z_2.

Both numerically found two-ψ_+ soliton solutions are plotted in Fig.6. For the sake of comparison, we plot the linear combination $\psi_+(x+z) + \psi_+(x-z) - \psi_0$ for $z = z_1$ and z_3 in the same picture. In plotting these linear combinations we take z_1 and z_3 to be equal to their *numerically observed* values, and not the maxima of the corresponding two-soliton interaction potential.

As the driving strength, h, is decreased down to $h_{\text{thr}} = 0.3318065$ (which coincides with the threshold value for the one-soliton solution), the $\psi^3_{(++)}$ complex turns into the solution which can be interpreted as $\psi^3_{(--)}$. For our reference value of h, $h = 0.35$, the observed intersoliton separation is $2z_3 \approx 26.20$ while the variational method gives $2z_3 = 25.60$.

The threshold driving strength for the lowest orbit, $\psi^1_{(++)}$, lies significantly higher: $h'_{\text{thr}} = 0.336837$. Similarly to the higher orbit, the solution $\psi^1_{(++)}$ transforms into the complex $\psi^1_{(--)}$. For $h = 0.35$, the variationally-predicted and numerically observed separations for this solution, are, respectively, $2z_1 = 4.85$ and $2z_1 \approx 5.60$.

Both "double-ψ_-" complexes are shown in Fig.7. On the same picture we plot the corresponding linear combinations $\psi_-\psi_-$ — for exactly the same values of the separation.

Finally, we also obtained the asymmetric two-soliton solution, $\psi_{(-+)}$. This complex "lives" at the third orbit and detaches from the corresponding $\psi^3_{(++)}$ and $\psi^3_{(--)}$ solutions at their merging point, $h = h_{\text{thr}} = 0.3318065$. At the reference point $h = 0.35$, the complex $\psi^3_{(-+)}$ has the orbital distance $2z_3 \approx 28.075$ whereas the potential of interaction has its third maximum at $2z_3 = 27.45$. This solution is presented in Fig.8. The linear superposition $\psi_-\psi_+$ is also shown for the sake of comparison.

Here we should mention a computational problem encountered in obtaining this asymmetric solution. For small h close to the turning point we were able to compute it with the residual $\delta \sim 10^{-8}$. However, as we moved in the direction of greater h, the convergence of our numerical algorithm deteriorated and we had to relax the residual. In particular, the portion of the asymmetric branch plotted by the dashed line in Fig.5, was computed with the residual $\delta \sim 10^{-6}$–10^{-5}. The separation value $2z_3 = 28.075$ in Table 1, was obtained with the residual $\delta = 0.5 \times 10^{-6}$.

We also have to mention here that we were not able to find the asymmetric solution living on the first (or second) orbit.

4.2 Three-soliton complexes

We now proceed to three-soliton associations. Two distinct "three-ψ_+" solutions detach from the flat background at the point $h = h_*$ (see Fig.5). The first solution has $z \approx 7.45$, and, comparing to the first maximum of the potential U_{eff} (which lies at $z = 7.925$), we identify it with the first orbit. The other solution has $z \approx 28.0$ whereas the third extremum of U_{eff} is at $z_3 = 28.425$. Consequently, this solution can be interpreted as the third orbit.

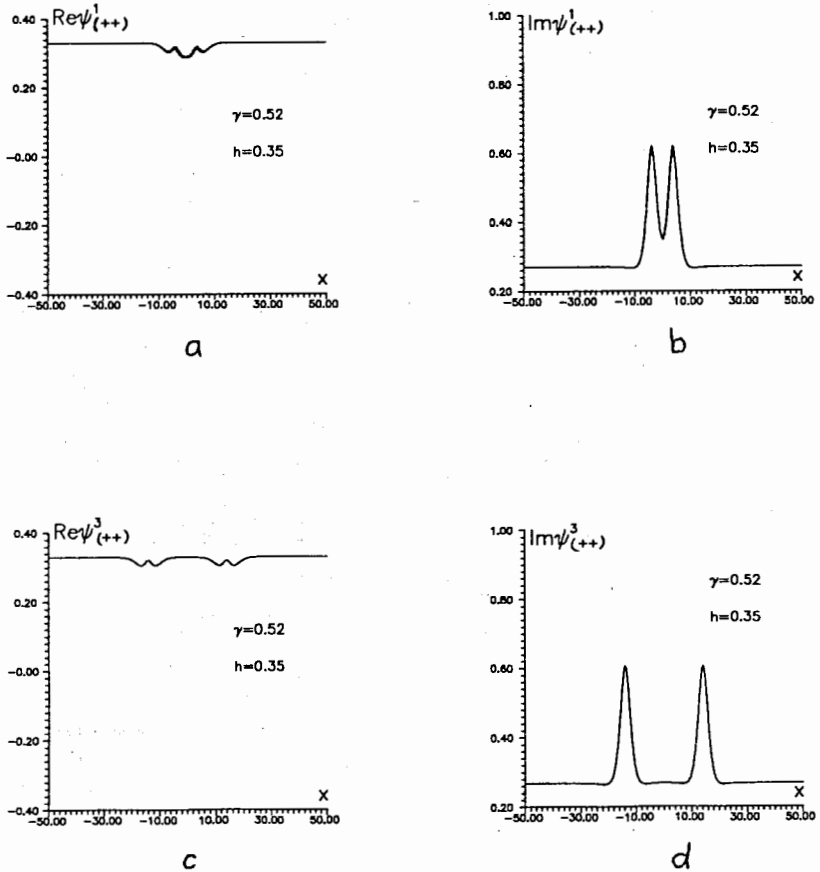

Fig.6 The $\psi_{(++)}$ solutions (solid line). a,b: the first orbit, $\psi^1_{(++)}$; c,d: the third orbit, $\psi^3_{(++)}$. For comparison, we also show the linear superposition $\psi_+\psi_+$ for the same value of the separation (dashed line). (On c,d the dashed and solid line are undistinguishable).

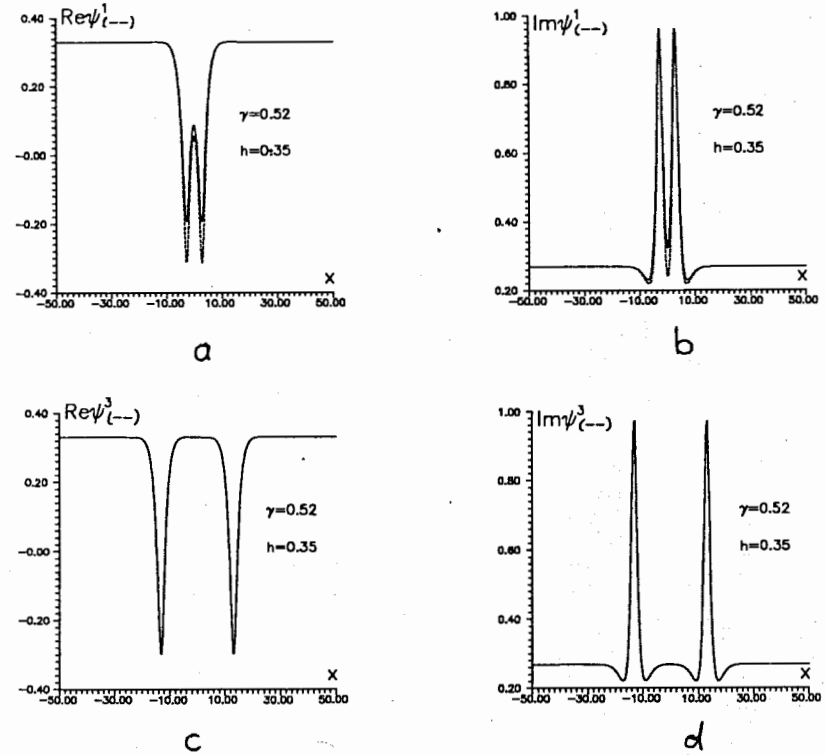

Fig.7 The $\psi_{(--)}$ complexes. a,b: the first orbit, $\psi^1_{(--)}$; c,d: the third orbit, $\psi^3_{(--)}$. For comparison, we also show the linear superposition $\psi_-\psi_-$ for the same value of the separation (dashed line).

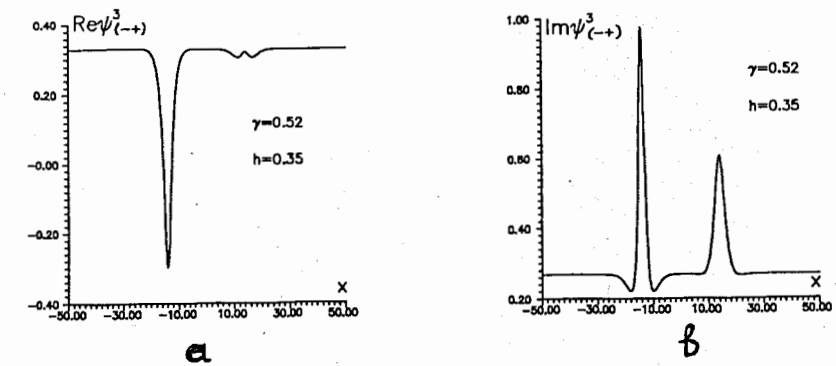

Fig.8 The $\psi^3_{(-+)}$ solution. On the same picture we tried to plot the linear combination $\psi_-\psi_+$ for the same value of the separation, but the two curves appear to be graphically indistinguishable.

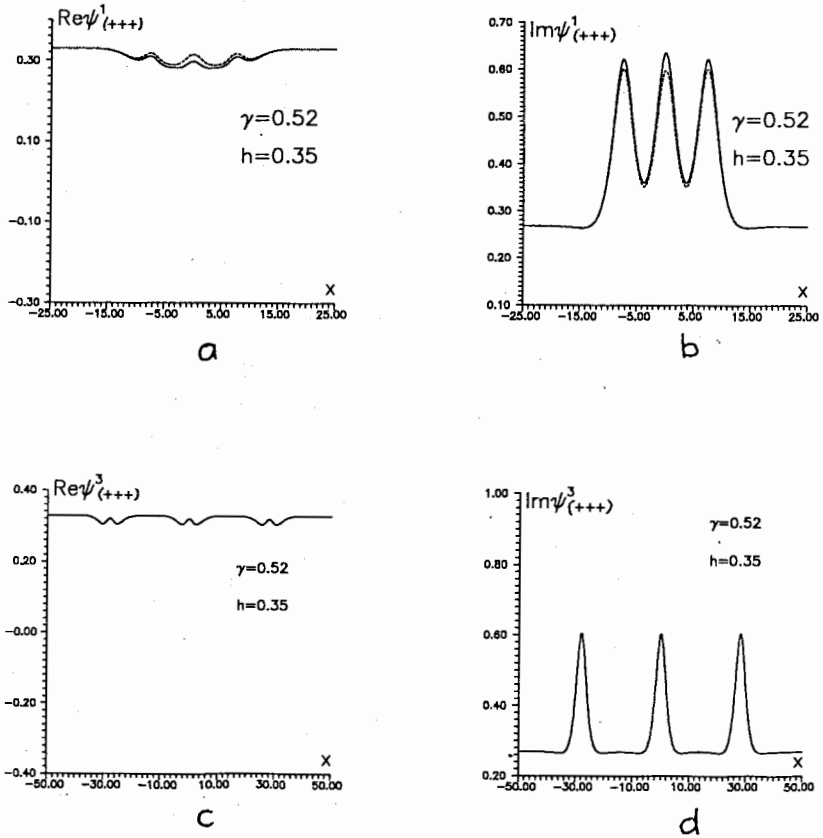

Fig.9 a,b: The $\psi^1_{(+++)}$ complex; **c,d**: the $\psi^3_{(+++)}$ solution. For comparison, we also show the linear superposition $\psi_+\psi_+\psi_+$ for the same values of the separation (dashed line).

Decreasing h from $h = h_*$ to the threshold value $h_{\rm thr} = 0.3318065$, the third orbit goes over to the $\psi^3_{(---)}$ solution (the uppermost curve in the bifurcation diagram Fig.5). At $h = 0.35$ the separation distance between the central and the side solitons, is $z_3 \approx 26.175$, which is in a reasonable agreement with the third extremum of $U_{\rm eff}$: $z_3 = 25.575$. Fig.10 displays this solution as well as another $\psi_{(---)}$ complex, to be described further on.

At the turning point $h_{\rm thr} = 0.3318065$ two more three-soliton branches are tangent to the $\psi^3_{(---)}$ - $\psi^3_{(+++)}$ curve. One of these is the $\psi^3_{(+-+)}$ complex which has $z \approx 25.05$. The fact that this solution can be identified with the complex $\psi^3_{(+-+)}$ follows from the comparison with the variational estimate which gives $z_3 = 27.50$ for the corresponding linear combination, and from the graphical comparison of the two configurations, Fig.11.

We have already encountered a collective state of the soliton ψ_- and two solitons ψ_+ in Sec.2; see Fig.3 e,f. However solitons constituting that complex had the separation distance $z \approx 14.80$ which is close to the *second* extremum of the corresponding interaction potential, $z_2 = 17.275$. Consequently, the multisoliton solution discussed in Sec.2 should be identified as the $\psi^2_{(+-+)}$ complex (i.e., the second orbit).

For those h where the second orbit was found, its energy is practically equal to the energy of the corresponding third orbit, $\psi^3_{(+-+)}$. (For this reason the two curves merge into one in Fig.5.) However the two orbits are different in their respective domains of existence: we were unable to continue the branch $\psi^2_{(+-+)}$ to the left of the value $h \approx 0.3465$ whereas the complex $\psi^3_{(+-+)}$ exists all way to the the turning point $h_{\rm thr} = 0.3318065$ (see Fig.5).

At the turning point $h_{\rm thr}$, the $\psi^3_{(+-+)}$ solution transforms into the $\psi^3_{(-+-)}$ complex. The latter collective state has $z_3 \approx 28.75$, with the variational estimate giving $z_3 = 27.50$. The corresponding profiles are plotted in Fig.12.

The above four three-soliton collective states "live" at the third orbit. We have also found the corresponding first-orbit complexes, $\psi^1_{(+++)}$, $\psi^1_{(---)}$, $\psi^1_{(+-+)}$, and $\psi^1_{(-+-)}$. The $\psi^1_{(---)}$ branch (see Fig.10 a,b) is the second branch from the top in Fig.5. The numerically observed solution has the separation $z_1 \approx 5.95$ while the variational estimate is $z_1 = 4.70$. At $h'_{\rm thr} = 0.339644$ it turns into the $\psi^1_{(-+-)}$ solution, plotted in Fig.12 a,b. The observed separation is $z_1 \approx 8.80$ while the variational estimate is $z_1 = 7.15$.

The $\psi^1_{(+++)}$ branch (see Fig.9 a,b) detaches from the flat solution; it has $z_1 \approx 7.45$, with the variational estimate being $z_1 = 7.925$. At the point $h'''_{\rm thr} = 0.341612$ it turns into another three-soliton first-orbit complex which deserves a special comment.

The solution in question has a shape similar to an ice-cream cone (fig.13.) It is not quite obvious whether this solution should be identified with the $\psi^1_{(+-+)}$ or $\psi^1_{(---)}$ complexes. In order to make the accurate identification, we compare the numerically found "ice-cream cone" solution with the linear combinations $\psi_+\psi_-\psi_+$ (Fig.13 a,b) and $\psi_-\psi_-\psi_-$ (Fig.13 c,d). Graphically, the $\psi_+\psi_-\psi_+$ seems to provide a better approximation. This indicates that the "ice-cream cone" should be identified with the $\psi^1_{(+-+)}$ complex. Another indication comes from the relation between the energies of the first-orbit complexes. Since the ψ_- soliton is "more energetic" than ψ_+, it is natural to expect the energies to relate as $E^1_{(+++)} < E^1_{(+-+)} < E^1_{(-+-)} < E^1_{(---)}$. This relation between the energies of the numerically obtained first orbits is achieved only if the "ice-cream cone" is identified with the $\psi^1_{(+-+)}$.

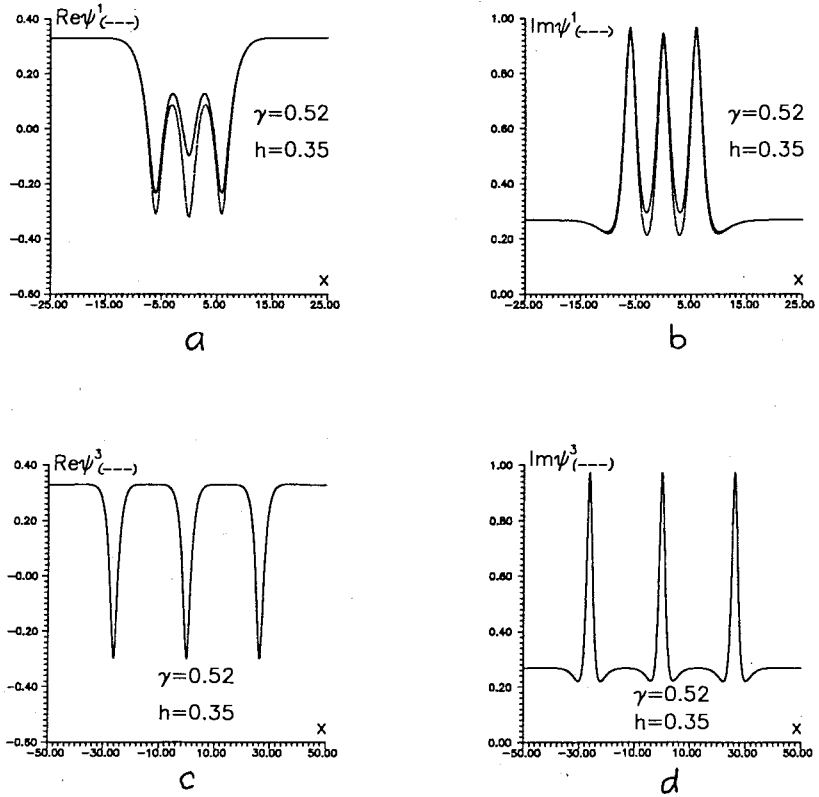

Fig.10 a,b: the $\psi^1_{(---)}$ solution; c,d: the $\psi^3_{(---)}$ complex.

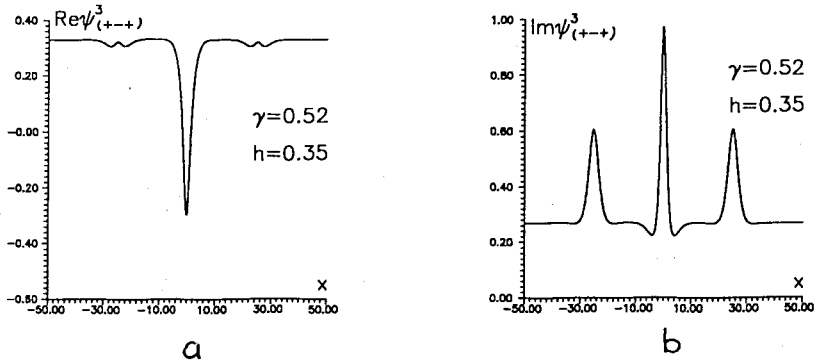

Fig.11 The $\psi^3_{(+-+)}$ complex.

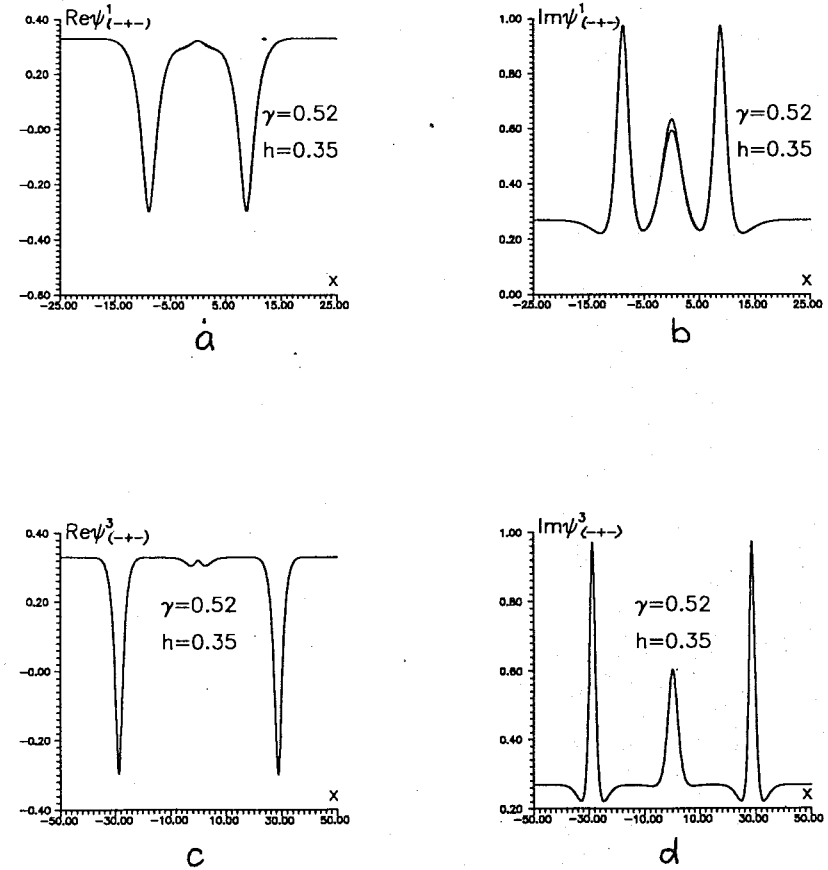

Fig.12 a,b: the $\psi^1_{(-+-)}$ solution; c,d: the $\psi^3_{(-+-)}$ complex.

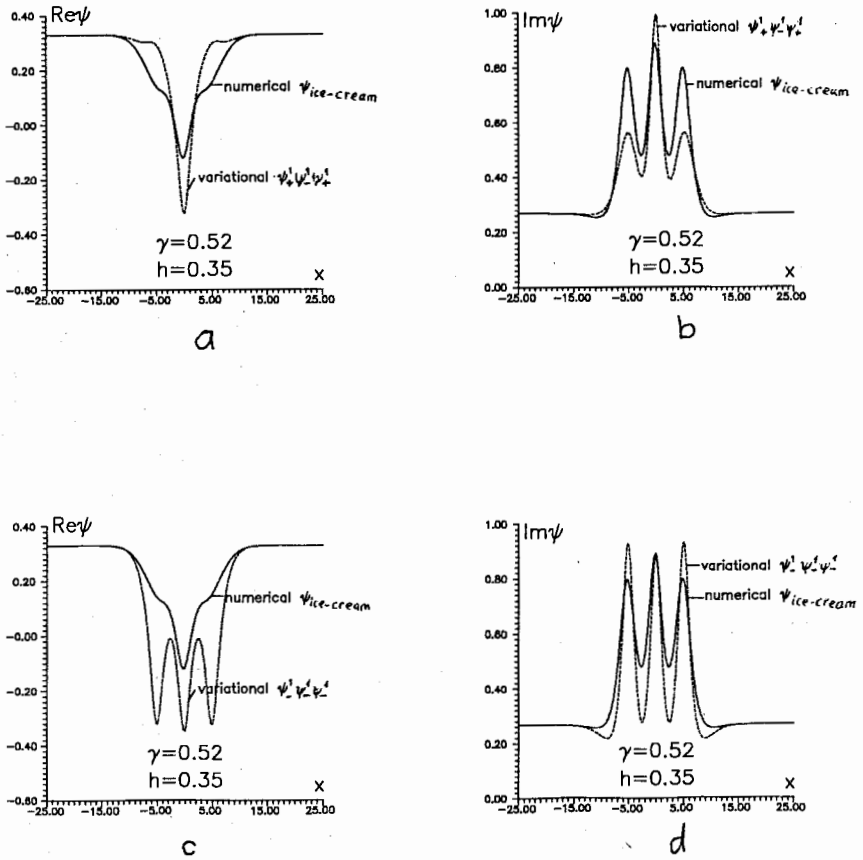

Fig.13 The ice-cream cone complex as compared with the $\psi_+\psi_-\psi_+$ (a,b) and $\psi_-\psi_-\psi_-$ (c,d) linear combinations.

5 Concluding remarks and open problems

1. A striking feature of the bifurcation diagram Fig.5 is almost the total absence of second-orbit complexes predicted by the variational approach. For example, the potential of interaction of two ψ_- solitons has two maxima, at $2z_1 = 4.85$ and $2z_3 = 25.60$, respectively, and a minimum in between, at $2z_2 = 15.35$ (see Table 1). However, despite all our attempts, we did not succeed in obtaining the complex $\psi^2_{(--)}$ by means of our Newtonian iterative algorithm. A similar situation occurred for most of the second-orbit complexes: the only exception was the $\psi^2_{(+-+)}$ solution.

A natural question is, therefore, whether these second orbits are really suppressed by some exclusion principle or is this simply a consequence of a deficiency of our numerical scheme. In order to check on this, direct numerical simulations of the full time-dependent NLS (2) were carried out, with the initial condition in the form of two ψ_- solitons at the distance of approximately $2z_2$ from each other. The formation of the stable bound state $\psi^2_{(--)}$ was indeed observed in these simulations [15]. (It is worth noting here that the $\psi^2_{(--)}$ complex had also been observed for stronger dampings, $\gamma = 0.6$. See [8].) Thus we still need to understand what prevents this and other second-orbit complexes from the numerical detection within the *stationary* NLS equation (3).

2. It is interesting to compare the soliton separations as predicted by the perturbative formula (45) with positions of the extrema of the potential $U_{\rm eff}$ obtained by the calculation of the energy of two- and three-soliton linear combinations, and with the actual separations of solitons in the numerically found multisoliton complexes. (That is, to compare the third, second and first columns in Tables 1 and 2.) As it could have been expected, the percentage error in the approximate results decreases as one proceeds from lower to higher orbits and the linear combination approximation becomes more adequate.

There is a very good agreement between the perturbative values (45) and positions of extrema of $U_{\rm eff}$ for complexes made up of ψ_- solitons only ($\psi_{(--)}$ and $\psi_{(---)}$). The agreement is worse for complexes involving solitons ψ_+. For example, the perturbative value for the third orbit is $5\pi/(2k) = 25.601$ while the full variational results for the $\psi^3_{(---)}$, $\psi^3_{(+-+)}$ and $\psi^3_{(+++)}$ complexes are 25.575, 27.50 and 28.425, respectively. The deterioration of the agreement for complexes involving ψ_+ is due to a weaker localization of the ψ_+ solitons in the neighbourhood of the point $h = h_*$.

Finally, we need to mention that for the complexes of the ψ_- solitons sitting on the first orbits ($\psi^1_{(--)}$ and $\psi^1_{(---)}$), the perturbative formula (45) gives a somewhat more accurate result than the full variational approach. (See Tables 1 and 2.) The nature of this phenomenon has remained unclear. One possible explanation could be that the relation (45) between the asymptotic wavenumber and separation distance is deeper than the explicit perturbative expression for the soliton which was used in its derivation.

3. We mentioned several other computational problems that we faced and that are still awaiting their resolution. These include the continuation of the asymmetric $\psi^3_{(-+)}$ solution in the direction of higher h and the continuation of the $\psi^2_{(+-+)}$ branch towards smaller h.

4. With a single exception of the $\psi^3_{(-+)}$ complex, we did not discuss asymmetric two and three-soliton collective states. We expect asymmetric branches to detach from symmetric complexes at all five turning points. For example, the $\psi^3_{(-++)}$ and $\psi^3_{(--+)}$ branches should

Table 1

	$2z_1$ num.	$2z_1$ var.	$\pi/2k$	$2z_2$ num.	$2z_2$ var.	$3\pi/2k$	$2z_3$ num.	$2z_3$ var.	$5\pi/2k$
$\psi_{(++)}$	7.60	7.95	5.120	-	18.20	15.361	28.00	28.45	25.601
$\psi_{(--)}$	5.60	4.85	5.120	-	15.35	15.361	26.20	25.60	25.601
$\psi_{(-+)}$	-	7.90	5.120	-	17.20	15.361	28.075 *)	27.45	25.601

Table 2

	z_1 num.	z_1 var.	$\pi/2k$	z_2 num.	z_2 var.	$3\pi/2k$	z_3 num.	z_3 var.	$5\pi/2k$
$\psi_{(+++)}$	7.45	7.925	5.120	-	18.175	15.361	28.00	28.425	25.601
$\psi_{(---)}$	5.95	4.70	5.120	-	15.325	15.361	26.175	25.575	25.601
$\psi_{(+-+)}$	5.02	6.925	5.120	14.80	17.275	15.361	25.05	27.50	25.601
$\psi_{(-+-)}$	8.80	7.15	5.120	-	17.275	15.361	28.75	27.50	25.601

Table 1 and 2. The intersoliton separations for the two- and three-soliton collective states. In each of the three cases, z_1, z_2 and z_3, the first column is the separation distance for the numerically obtained solution and the second column is its variational approximation. For comparison we also produce the corresponding prediction of the perturbative formula (45) with k given by Eq.(13). In both tables $h = 0.35$; all calculations were done on the interval $(-100, 100)$ using a sixth-order iterative algorithm with the step $\Delta x = 0.025$ and residual value $\delta \sim 10^{-8}$. The exception is *) where the residual was $\delta = 0.5 \times 10^{-6}$.

emerge from the quartic turning point, where $\psi^3_{(+++)}$, $\psi^3_{(+-+)}$, $\psi^3_{(-+-)}$, and $\psi^3_{(---)}$ solutions meet.

5. The bifurcation diagram Fig.5 is incomplete without understanding of how all multisoliton branches are connected. We have demonstrated, numerically, that the ψ_- solution continues as the $\psi^2_{(+-+)}$ complex. It is natural to expect more mergers between various pairs (or groups) of branches in a neighbourhood of the point $h = h_*$. We speculate that the process of proliferation of soliton complexes always occurs via the "addition" of low-energetic, small-amplitude ψ_+ solitons in the vicinity of h_*. Details of this transformation are still to be clarified.

6. When compiling the existence chart for the ac-driven damped NLS equation, we have identified two characteristic regions of γ values, $\gamma < 1/2$ and $\gamma > 1/2$ [10]. In the latter region (which the present paper was devoted to), solitons have oscillatory tails and this gives rise to an oscillatory potential of interaction, whose extrema correspond to stationary collective states. As we have already mentioned, the proliferation of multisoliton states occurs via the attachment of low-energetic, small-amplitude ψ_+ solitons near the value of h where the ψ_+ soliton merges with the flat solution. (This point corresponds to the upper boundary of the domain of existence of the ψ_+.) In the former region, neither ψ_+ nor ψ_- solitons have oscillatory tails in the vicinity of the merger point — yet multisoliton complexes were observed in computer simulations for $\gamma < 1/2$ [9]. It would therefore be interesting to find out what is the mechanism of their proliferation in that region.

7. Another open question is the multisoliton states' stability and lifetime. The variational two-particle approximation yields a sequence of equilibrium soliton separations, the first one corresponding to a maximum in their interaction potential $U_{\rm eff}$, second to a minimum, and so on. Consequently, one could expect that at least for small dampings, the first and third orbits will be unstable while the second one will have a finite lifetime due to dissipative losses [8]. However, direct numerical simulations do not always support this intuitively appealing idea. A suitable counterexample comes from the work of Wabnitz [9] who examined the case of $\gamma = 0.360$ and $h = 0.234$. In this case the soliton's asymptotic value is $|\psi_0|^2 = 0.061$, the asymptotic wavenumber $k = 0.190$ and the perturbative results (45) for the first two extrema of $U_{\rm eff}$ (the maximum and minimum, respectively), are $2z_1 = 8.26$ and $2z_2 = 24.78$. On the other hand, the simulations of Ref.[9] revealed a stable stationary soliton doublet with the separation distance $2z \approx 8$. Contrary to what one could have expected from the fact that this bound state is stable, it obviously corresponds to the *maximum* of the interaction potential (i.e. it should be identified with the $\psi^1_{(--)}$ complex.)

8. The fact that some of the multisoliton states may prove to be unstable, does not mean they would play no role in the soliton dynamics. Numerical simulations indicate that some *temporally-periodic* solitons have a spatial structure similar to the first-orbit two and three-soliton complexes [16, 17] and so the soliton collective states may happen to provide a better starting point for the perturbative or variational construction of time-dependent solutions. Another reason to keep an eye on the unstable states comes from the fact that they will be visited by *chaotic* attractors. Multihump structures were indeed observed in simulations of chaotic regimes in the damped driven sine-Gordon and NLS equations [11, 16, 17].

Acknowledgments. We benefited from discussions with M.M. Bogdan and B.A. Malomed. Authors thank Prof I.V. Puzynin and Prof C. Brink (University of Cape Town) for their support and assistance with research resources. Special thanks are to N. Alexeeva who

plotted Fig.4 for us. This research was supported by the FRD of South Africa, the University Research Council of the University of Cape Town. The work of the second author was also supported in part by the Russian Foundation for Basic Research (Grant #97-01-01040).

References

[1] D. J. Kaup and A. C. Newell, Phys. Rev. **B18** (1978), 5162;

[2] J.C. Eilbeck, P.S. Lomdahl, and A.C. Newell, Phys. Lett. A **87**, 1 (1981); P.S. Lomdahl and M.R. Samuelson, Phys. Rev. A **34**, 664 (1986);

[3] G. Wysin and A.R. Bishop, Journ. Magnetism and Magnetic Materials **54-57**, 1132 (1986)

[4] K. Nozaki and N. Bekki, Phys. Rev. Lett. **50** (1983), 1226; Phys. Lett. **102A** (1984), 383; J. Phys. Soc. Jpn. **54** (1985), 2363

[5] K. Nozaki and N. Bekki, Physica D **21**, 381 (1986)

[6] L.A. Lugiato and R. Lefever, Phys.Rev.Lett. **58**, 2209 (1987); M. Haelterman, S. Trillo, and S. Wabnitz, Opt.Lett. **17**, 745 (1992); Opt. Commun. **91**, 401 (1992).

[7] B. A. Malomed, Phys. Rev. **A44** (1991), 6954; Phys.Rev. E **47**, 2874 (1993)

[8] D. Cai, A. R. Bishop, N. Grønbech-Jensen, B. A. Malomed, Phys.Rev. E **49**, 1677 (1994)

[9] S.Wabnitz, Opt.Lett. **18**, 601 (1993)

[10] I.V. Barashenkov, and Yu.S. Smirnov, Phys.Rev. E **54**, 5707 (1996)

[11] A. R. Bishop, M. G. Forest, D. W. McLaughlin, and E. A. Overman, Physica D **23**, 293 (1986)

[12] G. Terrones, D.W. McLaughlin, E.A. Overman, A.J. Pearlstein, SIAM J. Appl. Math. **50**, 791 (1990)

[13] I.V. Barashenkov, M.M.Bogdan, and T. Zhanlav. In *Nonlinear World: IV International Workshop on Nonlinear and Turbulent Processes in Physics. Kiev, 9-22 October 1989.* V.G.Bar'yakhtar *et.al.*, eds. World Sci., Singapore (1990), p.3

[14] V.I. Karpman and S.S. Solov'ev, Physica D **3**, 487 (1981)

[15] N.V. Alexeeva, I.V. Barashenkov, and Yu.S. Smirnov, submitted for publication along with the present paper.

[16] K. H. Spatschek, H. Pietsch, E. W. Laedke and Th. Eickermann. In: *Singular Behaviour and Nonlinear Dynamics.* T. Bountis and St. Pnevmatikos, eds. World Sci., Singapore (1989)

[17] M. Bondila, I.V. Barashenkov and M.M. Bogdan, Physica D **87**, (1995), 314.

Received by Publishing Department
on April 2, 1997.

Барашенков И.В., Смирнов Ю.С. E5-97-111

Коллективные состояния солитонов нелинейного уравнения Шредингера с внешней накачкой и диссипацией

Изучены бифуркации локализованных стационарных решений нелинейного уравнения Шредингера с внешней накачкой и диссипацией

$$i\Psi_t + \Psi_{xx} + 2|\Psi|^2\Psi = -i\gamma\Psi - h e^{i\Omega t},$$

в области больших γ ($\gamma > 1/2$). Для каждой пары h и γ имеются два совместно существующих солитона Ψ_+ и Ψ_-. С увеличением мощности накачки h при фиксированном значении параметра γ солитон Ψ_+ сливается с плоским фоновым решением, а Ψ_- образует стационарное коллективное состояние с двумя «пси-плюсами»: $\Psi_- \to \Psi_{(+-+)}$. Также получены другие стационарные решения, и они идентифицированы как мультисолитонные комплексы $\Psi_{(++)}$, $\Psi_{(--)}$, $\Psi_{(-+)}$, $\Psi_{(---)}$, $\Psi_{(-+-)}$ и т.д. Соответствующие расстояния между солитонами сравниваются с расстояниями, полученными при использовании вариационной аппроксимации.

Работа выполнена в Лаборатории вычислительной техники и автоматизации ОИЯИ.

Препринт Объединенного института ядерных исследований. Дубна, 1997

Barashenkov I.V., Smirnov Yu.S. E5-97-111

Collective States of Externally Driven, Damped Nonlinear Schrödinger Solitons

We study bifurcations of localized stationary solitons of the externally driven, damped nonlinear Schrödinger equation

$$i\Psi_t + \Psi_{xx} + 2|\Psi|^2\Psi = -i\gamma\Psi - h e^{i\Omega t},$$

in the region of large γ ($\gamma > 1/2$). For each pair of h and γ, there are two coexisting solitons, Ψ_+ and Ψ_-. As the driver's strength h increases for the fixed γ, the Ψ_+ soliton merges with the flat background while the Ψ_- forms a stationary collective state with two «psi-pluses»: $\Psi_- \to \Psi_{(+-+)}$. We obtain other stationary solutions and identify them as multisoliton complexex $\Psi_{(++)}$, $\Psi_{(--)}$, $\Psi_{(-+)}$, $\Psi_{(---)}$, $\Psi_{(-+-)}$ etc. The corresponding intersoliton separations are compared to predictions of a variational approximation.

The investigation has been performed at the Laboratory of Computing Techniques and Automation, JINR.

Preprint of the Joint Institute for Nuclear Research. Dubna, 1997